Estuarine, Coastal and Shelf Science 215 (2018) 229–240

Contents lists available at ScienceDirect

Estuarine, Coastal and Shelf Science

journal homepage: www.elsevier.com/locate/ecss

Distribution of dissolved methane and nitrous oxide in Chilean coastal systems of the Magellanic Sub-Antarctic region (50°–55°S)

Laura Farías[a,b,*], Estrella Bello[a], Gresel Arancibia[c,d], Josseline Fernandez[c]

[a] Departamento de Oceanografía, Facultad de Ciencias Naturales y Oceanográficas, Universidad de Concepción, Chile
[b] Centro de Ciencia del Clima y Resiliencia (CR)^2, Chile
[c] Escuela de Ciencias del Mar, Pontificia Universidad Católica de Chile, Chile
[d] Servicio Nacional de Pesca, Chile

ARTICLE INFO

Keywords:
Methane
Nitrous oxide
Chilean fjords
Magellanic sub-antarctic region

ABSTRACT

Nitrous oxide (N_2O) and methane (CH_4) are greenhouse gases and active in the depletion of the ozone layer. These gases, originating from both anthropogenic and natural sources, are mainly released to the atmosphere from coastal areas, including continental shelves, estuaries and fjords. Surface distribution of dissolved N_2O and CH_4 during the austral spring were described within the Magellanic Sub-Antarctic region (50–55°S, Chile) with a coastal area that has a complex system of fjords, channels, gulf and, bays. A narrow range of N_2O concentrations were observed from under-saturations (~65%), as result of freshwater/glacial flow into fjord heads, to slight super-saturations (~120–150%) in fjord mouths and adjacent marine zones. One exception was Otway Sound, where a penguin colony is situated, with N_2O levels of up to 218%. In contrast, CH_4 concentrations presented a wide range of saturations between 47.9% and 483%, with a spatial distribution that mainly corresponded to the type of hydrographic/geomorphologic basin; in the southern Patagonian Andes (mostly covered by the southern Ice Fields) CH_4 levels varied between 65 and 80% in the marine area, and 180% saturation in the channels and fjords; whereas in the southern Patagonian tableland (Magellan Strait) higher CH_4 concentrations, up to 483% saturation, were observed apparently associated with continental inputs (peatland and tundra vegetation). N_2O concentrations were positively correlated with salinity and nutrients, indicating that the majority of N_2O and nutrients (except silicate) originated from the Sub-Antarctic Water Mass (SAAW), which mixes with N_2O-depleated freshwater. However, CH_4 concentrations did not correlate with any oceanographic variables, suggesting that they originate from local marine/terrestrial interactions. The Magellanic Sub-Antarctic region acts as a modest source of N_2O and CH_4, to the atmosphere with effluxes of 6.20 ± 10.13 and $16.88 \pm 27.04\ \mu mol\ m^{-2}\ d^{-1}$ respectively. Due to climate change and a growth in anthropogenic activities such as salmon farming, future emissions of N_2O and CH_4 within this remote region remain uncertain.

1. Introduction

Nitrous oxide (N_2O) and methane (CH_4) are both active gases causing direct (greenhouse gas) and indirect (radiative) forcing in the troposphere and stratosphere (Portmann et al., 2012). The atmospheric concentration of both gases has increased at differing rates since the industrial revolution, as a product of both natural and anthropogenic sources (IPCC, 2013). The balance between sources and sinks of these gases determines the global N_2O and CH_4 budget. Whereas N_2O comes mainly from biogenic sources mainly associated with agricultural activities, as well as from the combustion of fossil fuels and solid waste CH_4 sources originate from biogenic (wetlands, lakes, agriculture, waste, landfill, permafrost), thermogenic (fossil fuel usage, hydrates and natural seeps) and pyrogenic (biomass and biofuel burning) sources (US EPA, 2010).

There is considerable uncertainty in the size of reservoirs and fluxes of both gasses (Ciais et al., 2013). For N_2O, soils are the main natural source (55%) followed by oceans (25%) (Nevison et al., 1995; US EPA, 2010); while wetlands are the dominant sources of CH_4, (63%) with inland waters and oceans contributing only 11.5% and 5%, respectively of the total natural emissions (Kirsche et al., 2013; Saunois et al., 2016). Additionally, the rate of gas exchange across the air-sea interface is not homogenous in the oceans, and most N_2O and CH_4 emissions originate from coastal sources; including estuaries, continental shelves and upwelling systems. Indeed, coastal areas may be responsible for ca. 75% of the CH_4 (Bange et al., 1994; Holmes et al., 2000; Borges and Abril,

* Corresponding author. Departamento de Oceanografía, Facultad de Ciencias Naturales y Oceanográficas, Universidad de Concepción, Chile.
E-mail addresses: laura.farias@udec.cl, lfarias159@gmail.com (L. Farías).

https://doi.org/10.1016/j.ecss.2018.10.020
Received 12 June 2018; Received in revised form 7 October 2018; Accepted 26 October 2018
Available online 28 October 2018
0272-7714/

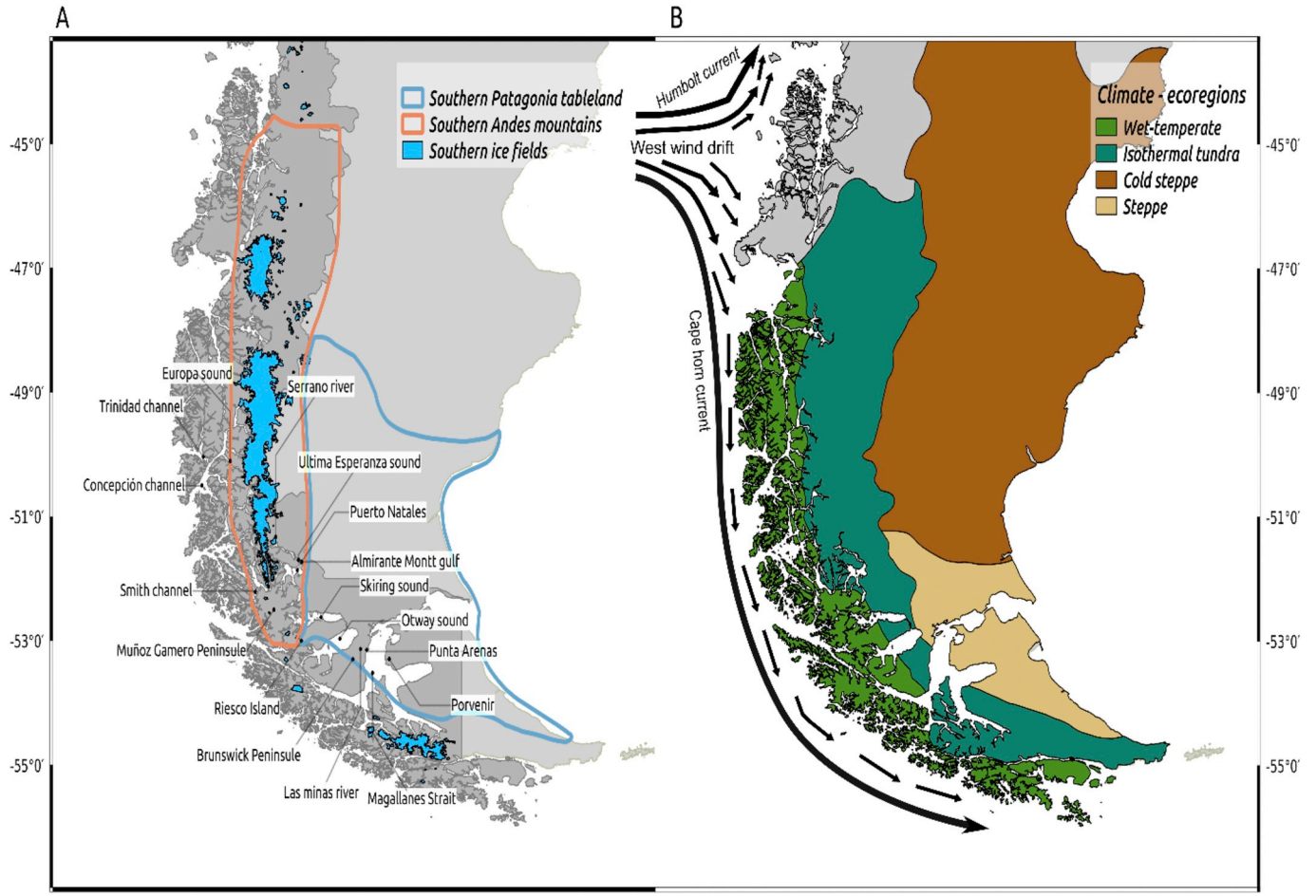

Fig. 1. Map of Patagonia showing: (a) geomorphology, including geographic place and (b) climate regimen including ocean currents superimposed on the area of the Magellanic region. Shaded and cracked areas correspond to the oversimplification of two types of geological structure and major hydrographic basins draining into the Pacific. The main fjords, channels or others features of the region are indicated.

2011), and ca. 32% of the N_2O (Nevison et al., 2004; Denman et al., 2007) global oceanic emissions.

Gas content in surface waters and exchange with the atmosphere is primarily driven by physical and biogeochemical processes (Suntharalingam and Sarmiento, 2000). Physical processes include changes in gas solubility (dependent on temperature and salinity), and gas distribution in the water column related to the redistribution of gas through circulation, stratification and mixing/turbulent processes. . Fjords present a marked hydrographical variability, related to freshwater input from tributary rivers and others, generating significant variations in salinity and resulting in stratification of the water column which drives typical estuarine circulation (Cameron and Pritchard, 1963). Additionally, in polar and sub-polar coastal areas, gas distribution effected by sea ice and glacial freezing and melting cycles should also be considered (Kiditis et al., 2010; Randall et al., 2012; Damm et al., 2015).

N_2O and CH_4 yields are highly dependent microbial activity, controlled by the dissolved oxygen concentration organic material availability (Reeburgh, 2007; Bange, 2010). In marine environments, N_2O is predominantly produced as a by-product of nitrification (conversion of NH_4^+, into NO_3^-) and partial denitrification (conversion of NO_3^- to N_2O). Nitrification is an aerobic process that occurs throughout global oceans as a part of the aerobic remineralization of organic matter (Bange, 2010). Unlike nitrification, CH_4 is produced predominantly through methanogenesis, an exclusively anaerobic process that is the final stage of anaerobic organic matter remineralization (occurring within anoxic sediment or the oxygen minimum zone) (Reeburgh, 2007). However, the supersaturation of CH_4 in oxygen-saturated near-surface waters is commonly observed as a result of CH_4 regeneration through organic methyl compounds (Karl et al., 2008; Carini et al., 2014).

This study focus on Magellanic Sub-Antarctic region, whose geomorphology is the combined effect of glacial erosion and the sinking of longitudinal valleys (Araya-Vergara, 2004), creating thousands of islands, peninsulas, channels and fjords and representing the most extensive fjord region in the world (Cameron and Pritchard, 1963) that exceeds 1.700 km (~40% Chile's length) from 42° to 56°S (Pantoja et al., 2011). The fjord hydrography consistently indicates a highly stratified buoyant surface layer with marine water located below; water circulation follows a basic estuarine flow pattern with less dense freshwater at the surface migrating towards the ocean and a deeper layer of denser oceanic water flowing towards the river source (Valdenegro and Silva, 2003). In addition, the southern Ice Field located in the southern Andes cordillera is rapidly decreasing in volume through large outlet glaciers, which thus increases the freshwater discharge into coastal zones (Willis et al., 2012). In this region, ice tongues extend into the dense fjord network, with tidewater calving glaciers occurring at sea level (Casassa et al., 2002). Oceanographically, at the sub-Antarctic Front (SAF), located between 48° and 58ºS, Sub-Antarctic Water (SAAW) is formed (Hartin et al., 2011). The SAAW migrates northward, absorbing and storing heat, freshwater (Holte et al., 2012; Karstensen et al., 2002), as well as entering the Patagonian fjords and mixing with fresh water from glaciers and rivers.

In addition, Magellanic Sub-Antarctic region has low anthropogenic

influences (population density around 3.3 habitant km^2). However, a growing salmon aquaculture industry (Buschmann et al., 1996) may detrimentally impact the environment and biomes. These activities could be important sources of N_2O and CH_4 to the atmosphere (Williams and Crutzen, 2010). Furthermore, seasonal changes in climate variables (e.g., solar radiation, wind, and precipitation) as well as different physical regimens (mixing and circulation in the water column) lead to complex marine/terrestrial interactions (Iriarte et al., 2016), which could potentially be affected by climate change (Gille, 2002). For example, the SAF, which is highly sensitive the westerly wind belt, is showing some latitudinal shifts as product of changes in atmospheric and oceanographic circulation (Thompson and Solomon, 2002; Oke and England, 2004; Fyfe et al., 2007).

2. Methods

2.1. Geological, climate and hydrology of the study site

The study area is presented in Fig. 1, highlighting major geographical formations, human activity and surface currents the Magellanic Sub-Antarctic region. Geomorphologically and geographically, the area comprises the southern Patagonia Andes and the Magellan tableland or "meseta" (Fig. 1b) conforming two hydrographic basins, the Pacific Ocean and the Magellan slope, respectively (Coronato et al., 2008). Part of the southern Andes region overlaps with the southern Patagonia Ice Field, considered to be the third largest fresh water reserve globally (Naruse and Aniya, 1992). This Ice Field extends approximately 350 km, from 48°15′ S to 51°30′ S, over an area of 12.363 km^2. Approximately 9.700 km^2 of this area is contained within the Pacific side (Chile) and it is rapidly losing mass through major outlet glaciers (Willis et al., 2012). Additionally, the Andes range is positioned perpendicular to the westerly wind, generating a wet-temperate climate with a high rainfall of up to 5000 mm y^{-1} (Zamora and Santana, 1979) and supporting dense wet forests dominated by Nothofagus species. On the contrary, the Southern Patagonian tableland is situated to the south-east of the Andean Cordillera, including the Magellan Strait and part of the Fuegian archipelagos. South of 52°S, the altitude of the mountain range is reduced and loses continuity, merging with the "meseta". Towards the interior of the archipelago the climate is modified, becoming relatively less wet with an isothermal tundra (dominated by peat bogs composed of Sphagnum mosses) to the west and southwest of the Magellanic Sub-Antarctic region, and a cold steppe climate (dominated by grasses) to the eastern part of the Magellan strait and the Fueguin archipelagos, characterized by a more pronounced thermal amplitude and a relatively low rainfall respect to northern and central Patagonia.

In the Magellan Sub-Antarctic region, westerly winds drive that SAAW to penetrate into the channels and fjords; it mixes with freshwater from the continental runoff. This causes a reduction in salinity creating the modified Sub-Antarctic Waters (MSAAW), defined as lower salinity water mass (< 32) (Silva et al., 1998). In the southern Patagonia fjords, water circulation follows a two-layer estuarine flow pattern (Sievers and Silva, 2008); where brackish water moves out superficially, and marine water enters, predominantly through the gulfs and channels. Wind-associated and/or tidal effects can generate strong surface currents, particularly in narrow channels (Cáceres et al., 2003; Valle-Levinson et al., 2007).

2.2. Sampling

Continuous and discrete sampling was carried out throughout the CIMAR cruises (CIMAR, Marine Research Cruises in Remote Areas). Cimar 15 cruise (11th October-19th November 2009) took place onboard the RV AGOR 60 "Vidal Gormaz" from Canal Trinidad to the western Pacific side of the Magellan strait; Cimar 16 cruise (20th October 12th November 2010) took place onboard the B/I "Abate Molina" along the Magellan Strait (52°S) and Fueguin Archipelagos. The location of the sampling station, date of sampling and other features are included in Table S1. In addition, oceanographic data from adjacent marine areas was obtained during the Intermediate Water (AAIW) cruise (KN182-7), during August 23rd – October 4th, 2005 onboard the Knorr Vessel. Since all data were collected over a same season, the analysis may avoid the effect of seasonal thermal variations on gas solubility and biological processes occurring in sub-Antarctic region (Bouman et al., 2012).

Vertical profiles of temperature (T°C), salinity, water density (kg m^{-3}), and dissolved oxygen (μM) were obtained using a conductivity, temperature, depth and dissolved oxygen (membrane-type) sensors (CTDO) (SBE 911plus for the CIMAR cruises, and SBE25 for the KN182-7 cruise; SeaBird Scientific, USA). Seawater samples were collected using Niskin bottles (15 l) mounted in a rosette. Seawater samples for N_2O, CH_4 and nutrients, sampled in this order, were obtained from two depths (1 and 10 m) in the majority of sample stations. Four stations (St 43, 62, 75 and P) were selected for a more in depth analysis to measure gas and nutrient profiles over several depths (1, 5, 10, 25, 50, 75, 100 and 150 m). Water samples for N_2O and CH_4 were collected in triplicate for each depth (one Niskin bottle per depth), and into a 20 mL glass GC to overflow vials using a gastight tube, then immediately poisoned with $HgCl_2$ (0.1 mL of saturated $HgCl_2$ solution per vial). Subsequently, the vials were sealed with a butyl-rubber septum and an aluminum cap, and stored in darkness at room temperature (~18 °C) until laboratory analysis For CIMAR 15 and 16, samples for nutrient analysis (NO_3^-, soluble reactive phosphorous "SRP" and Si (OH) $_4$ were taken in high density polyethylene bottles (50 mL), fixed with 2 drops of diluted $HgCl_2$, and then frozen at −20 °C until laboratory analysis.

2.3. Chemical analysis

N_2O and CH_4 were analyzed via the headspace method, adding a 5 mL helium (UHP, LINDE, USA) headspace into the vial (McAulliffe, 1971) using a gas-tight syringe; and then equilibrating the gas and liquid phases within the vial at 40 °C and 25 °C in a stove, respectively. N_2O and CH_4 were quantified in the headspace using a SHIMADZU-17a gas chromatograph (GC) equipped with an electron capture detector (ECD), using an Ar/CH_4 gas mix as a carrier gas, with a flow of 6.5 mL min^{-1}, operated at 250 °C for N_2O and, equipped with a flame ionization detector (FID), using a N_2 (ultra pure, LINDE, USA) as carrier gas, at a flow of 4 mL min^{-1} through a GS-Q capillary column at 30 °C for CH_4.

The analytical error of the GC for N_2O and CH_4 analyses was less than 3% and 7%, respectively. Uncertainty was calculated with the standard deviation of the triplicate measurements for each depth. Samples with a variation coefficient greater than 10% were omitted from the gas database. The nutrient analysis was carried out using a nutrient autoanalyzer, following the colorimetric techniques described by Atlas et al. (1971). For the CIMAR 16 cruise, a SEAL autoanalyzer was used to measure NO_3^- and SRP, following (Grasshoff et al., 1983). Coefficient of variation for NO_3^{-1} and SPR was better than ± 10% and ± 3%, respectively, with detection limits of 0.1 and 0.04 μM, respectively. For the AAIW- KN182-7 cruise, an ODF-modified 4-channel Technicon AutoAnalyzer II was used following the colorimetric techniques reported by Bouman et al. (2012).

2.4. data analysis

Saturation percentages of N_2O and CH_4 were calculated from N_2O and CH_4 concentrations, using current annual estimates of gas concentrations in the atmosphere from NOAA, with respect to the sampling period. These saturation percentages were based on *in situ* temperature and salinity records, and adjusted to the N_2O and CH_4 solubility parameterization (Weiss and Price, 1980; Wiesenburg and Guinasso, 1979, respectively).

Air-seawater N_2O and CH_4 fluxes (F_{air}), in μmol day^{-1} m^{-2}, were estimated using the following equation:

$$F_{air} = k_w(C_w - C_{sat}) \quad (1)$$

where k_w (cm s^{-1}) is the gas transfer velocity depending on wind speed, C_w is the N_2O and CH_4 concentration (nM) in the sample, and C_{sat} is the N_2O and CH_4 concentration in equilibrium with the atmospheric concentrations, according to the solubility parameterization of Weiss and Price (1980) and Wiesenburg and Guinasso (1979), respectively. Calculations of k_w were made using the parameterization of Nightingale et al. (2000):

$$k_w = (9.25{\cdot}10^{-7}u + 6.17{\cdot}10^{-7}u^2)\left(\frac{Sc}{600}\right)^{-0.5} \quad (2)$$

where u is the wind speed at 10 m over sea surface (cm s^{-1}), and Sc is the Schmidt number. For N_2O and CH_4, the Schmidt number is a function of temperature (°C), as given by Wanninkhof (2014):

$$Sc = 2356.2 - 166.38{\times}T + 6.3952{\times}T^2 - 0.13422{\times}T^3 + 0.0011506{\times}T^4 \quad (3)$$

The parameterization of Nightingale et al. (2000) was compared with that of Liss and Merlivat (1986). The wind speed data was measured on board and normalized to 10 m height using relationship from Garratt (1977). Wind speed was estimated over a moving seven day average prior to the sampling period, in order to smooth out short-term fluctuations and highlight longer-term trends. In addition, Spearman rank correlations (Rho) between salinity, temperature, N_2O, CH_4, and nutrients were applied for data obtained at the surface (1 m) and 10 m depth. The threshold value for statistical significance was set at $p < 0.05$. Data were processed using Primer 6.0 (Quest Research Limited, NZ) and Sigma Stat 4.0 (Systat Software, USA). Spatial data were plotted using the Ocean Data View program 4.0 (UNESCO).

3. Results and discussion

3.1. Surface distribution of physical-chemical variables

Surface (1 m depth) temperature, salinity and O_2 distributions are shown in Fig. 2. The surface temperature fluctuated between 2.94 °C and 8.00 °C (mean ± SD = 6.53 ± 0.80) reaching minimum values at the head of Europa Sound (St. 39), as well as at other fjord heads (St. 72, St.74, St. 75, St. 51 and St. 53) adjoined to the Southern Ice Field. Maximum temperatures were observed in marine water, close to southwest Pacific Ocean (St. 44 and St. 14) (Fig. 2a). Surface salinity widely fluctuated, between 14.59 and 34.14 (mean ± SD = 29.92 ± 5.66). Minimum values were observed in the Ultima Esperanza Sound at St. 51 (a semi-enclosed basin with two narrow channels) that converges with other channels and flow into the Almirante Montt Gulf (Fig. 2b). There, freshwater discharge from the Serrano River (average annual flow of 61 m^3 s^{-1}) and others minor tributaries converge with outflow from the Ice Field, causing salinity decreases (Niemeyer and Cereceda, 1984). In contrast, salinity in the Inner Sea and Magellan strait was around 25 and higher than 29, respectively. Stations associated with the Strait of Magellan had significantly higher salinity than the southern Patagonia Cordillera basin. This was apparently due to the flow of Sub-Antarctic water masses from the Pacific and Atlantic Ocean, through the Magellan strait (Valdenegro and Silva, 2003). In addition, within the Patagonia Tableland there were mostly endorheic rivers, or rivers that run off into the Atlantic Ocean (Coronato et al., 2008); thus, in comparison with north and central Patagonia from 40° to 48°S, freshwater discharge was relatively more reduced in the Magellanic Sub Antarctic region (Dussaillant et al., 2012).

Dissolved O_2 concentration in the surface water fluctuated between 232 μM and 388 μM; these levels indicated high levels of oxygenation (mean ± SD = 322.32 ± 23.06 μM) (Fig. 2c). A T-S diagram was used to identify water masses present in the oceanic area adjacent to the austral region using data collected during the AAIW- KN182-7 cruise (Fig. 2d). The diagram revealed the presence of three water masses, all of them with high levels of oxygenation (> 150 μmol L^{-1}) (Llanillo et al., 2013; Carrasco et al., 2017). They are Subantarctic Water (SAAW), Antarctic Intermediate Water (AAIW) and North Pacific Deep Water (PDW) in the open area adjacent to the austral channel region, using data collected during the AAIW- KN182-7 cruise (Fig. 2d). An analysis of the southern zone showed that the SAAW and the AAIW entered into the channels and fjords. The SAAW originates north of the SAF, under the stormy conditions of the sub-polar low pressure systems, where high rates of precipitation markedly reduce the salinity of the surface layers being relatively fresh (~33.8) and with a temperate ~11.5 °C (Silva et al., 1998). Below the SAAW, the AAIW is found at 500–900 m and is formed by vertical convection of the deep winter mixed layer located north of the Polar Front having a salinity (< 34.5) (Hartin et al., 2011; Tsuchiya and Talley, 1998).

3.2. Surface distribution of greenhouse gases and nutrients

Surface N_2O concentration and its saturation with respect to the atmosphere are shown in Fig. 3. Dissolved N_2O concentration (considering 1 and 10 m depth) fluctuated between 7.88 and 26.4 nM (65%–218%), with a mean ± SD value of 14.7 ± 2.91 nM. Undersaturation was observed in Europa Sound, Ultima Esperanza Sound, and other sounds close to the Southern Ice Field (Fig. 3b), suggesting a potential dilution from melt water with low levels of gases. The occurrence of N_2O depletion had been observed in (sub)polar waters of the Arctic Sea (Randall et al., 2012; Verdugo et al., 2016) and in Southern Ocean close to Kerguelen island (Farías et al., 2015), due to the dilution of surface water from glacial and/or sea-ice melt (Rhee et al., 2009; Zhan et al., 2015). During the period of ice formation, bubbles include in the ice are expected to have a similar gas composition and concentration to the atmosphere, but during formation of firn (ice that is at an intermediate stage between snow and ice), gases flow to surrounding water bodies or are vented to the atmosphere, thus gas content within that ice is lower (Schwander et al., 2017). However, during spring-summer, ice melt dilutes water next to glacial and reduces the dissolved gas content, potentially triggering under-saturated conditions in the surrounding waters (Kiditis et al., 2010; Randall et al., 2012). The same pattern was observed for total alkalinity and dissolved inorganic carbon (DIC) which decreased as product of freshwater dilution observed near melting glaciers (Vargas et al., 2018). Indeed, riverine and ice melting DIC influenced the DIC pool in the southern Chilean Patagonia due to that DIC concentration from rivers and glaciers are relatively low.

On the contrary, increased N_2O was observed in the Otway sound (St. 21), a practically closed system situated on the Patagonian tableland. A penguin colony of ca.10.000 individuals, inhabit the Sound between September and March of each year. A fertile ornithogenic soil, consisting of Penguin guanos, is rich in organic carbon, nitrogen and phosphorus, which stimulates the cycling of gases containing C, N and S compounds, a key source of N_2O and CH_4 to the atmosphere/water (Sun et al., 2002). Conversely, N_2O levels in the Pacific Ocean, adjacent to southern Patagonia (49°-55°S) were almost in equilibrium with the atmosphere (100% or ~12 nM), or had lightly saturated conditions (~125% or ~15 nM) with respect to the atmosphere (Fig. 3). Similar results were reported by Carrasco et al. (2017), reporting an N_2O increase as the SAAW moves northward, from undersaturated conditions to the north of the polar front to slightly saturated conditions in offshore Patagonian waters.

The distribution and its saturation of surface dissolved CH_4 concentration is presented in Fig. 4. Dissolved CH_4 concentration (considering 1 and 10 m depth) ranged from 1.46 to 14.44 nM, corresponding from 49 to 483% saturation. There was not a clear spatial pattern of surface CH_4 distribution. In general, higher levels were observed in the Inner Sea compared to the open ocean (where

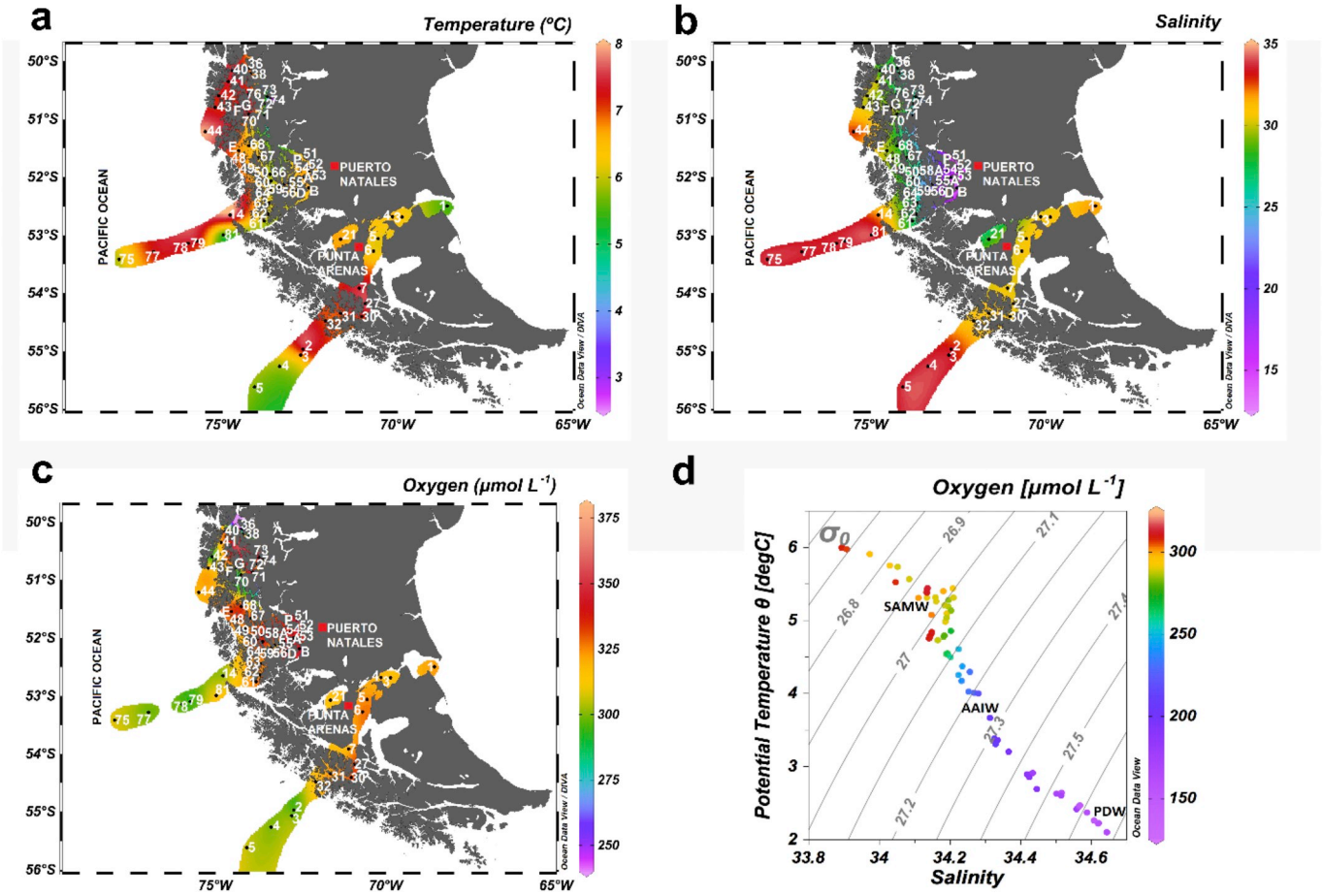

Fig. 2. Surface spatial distribution of **(a)** temperature, **(b)** salinity, **(c)** oxygen and **(d)** potential temperature-salinity diagram and oxygen color-coded. Water masses are indicated according their expected σ_Θ, basically the SAAW and modal SAAW, AAIW and CDW. Small dots indicate station. Ocean Data View gridding was applied. (For interpretation of the references to color in this figure legend, the reader is referred to the Web version of this article.)

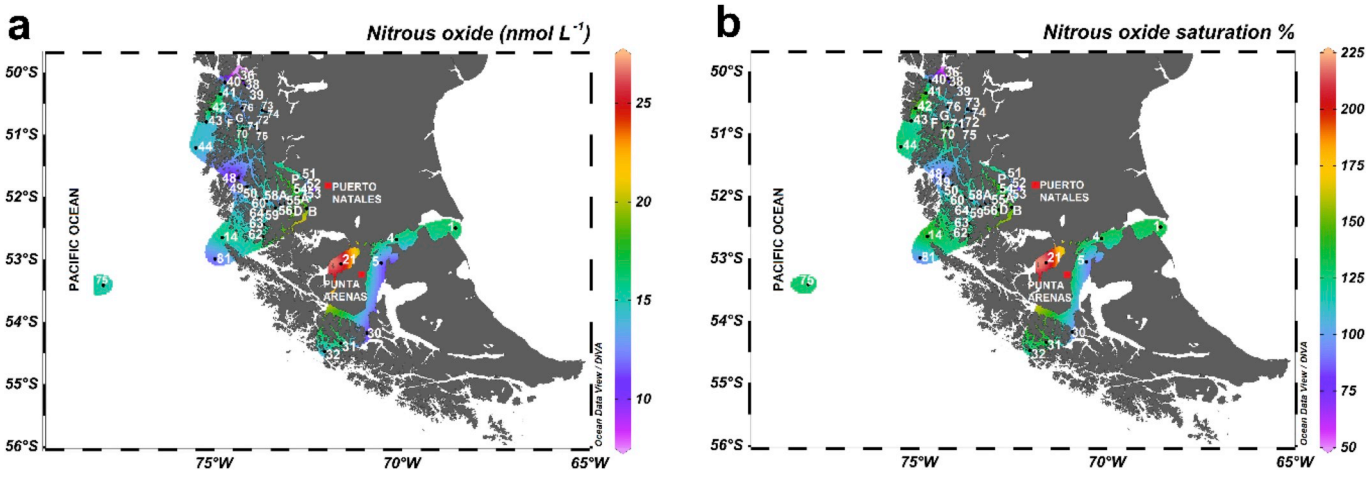

Fig. 3. Surface spatial distribution of: (a) nitrous oxide concentration (nM L^{-1}) and (b) its gas saturation condition (%) in the Magellanic region. Small dots indicate station and depth of the discrete samples. Ocean Data View gridding was applied.

undersaturated conditions were present), and the brackish waters in the heads of some fjords from the Europa and Ultima Esperanza sound (i.e., St, 51, St. 52, St. 53, St. A, St. B and St. D), located predominantly to the west of the southern Andes slope. By contrast, several CH_4 hotspots were observed in the Patagonian tableland; for example, St. 6 located close to Punta Arenas at the mouth of Las Minas River (DGA, 2012). Other CH_4 maxima were observed at the northwest part of Skiring Sound and Riesco island, including St. 60, St. 61, St. 63 and St. 64, with concentrations of ~13 nM, equivalent to ~420% (Fig. 4b).

High levels of CH_4 may be associated with the transfer of gas from soils to coastal areas via continental runoff. There may be naturally higher CH_4 production due to the presence of peatland as is found in the western sector of the Magellan strait. Peatland or wetlands that contain a large amount of peat (or partially decayed plant life), dominated by *Sphagnum*, are abundant in the Magellanic tundra, predominantly concentrated in the Muñoz Gamero peninsula, Riesco Island, and the

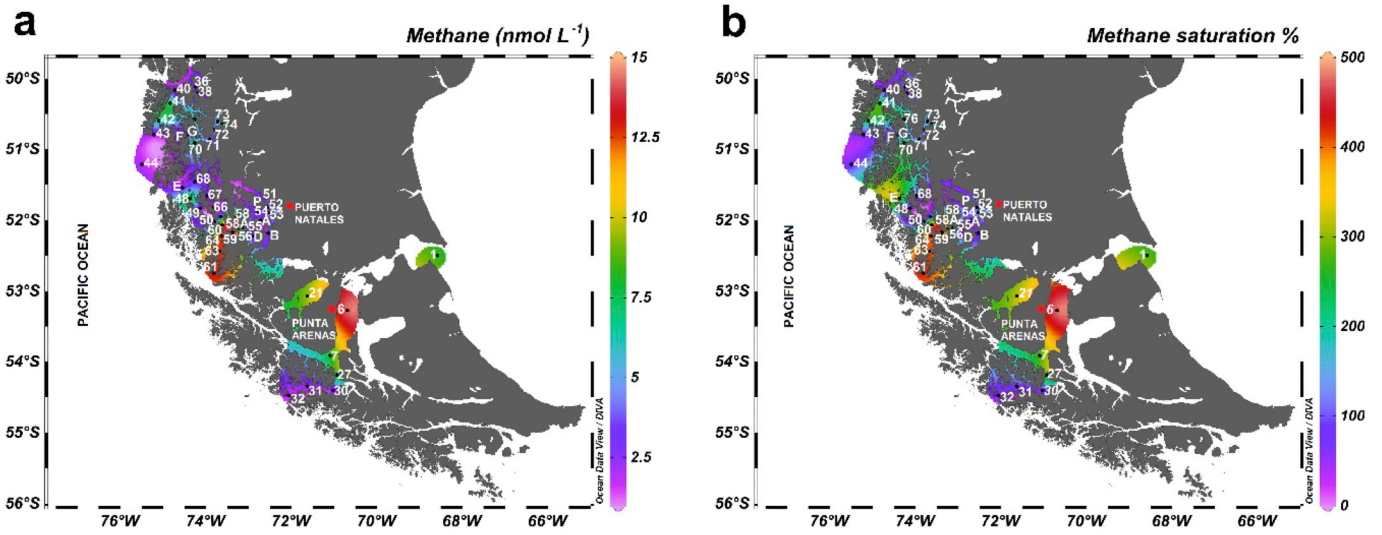

Fig. 4. Surface spatial distribution of: (a) methane concentration (nM L^{-1}) and (b) its gas saturation condition (%) in the Magellanic region. Small dots indicate station and depth of the discrete samples. Ocean Data View gridding was applied.

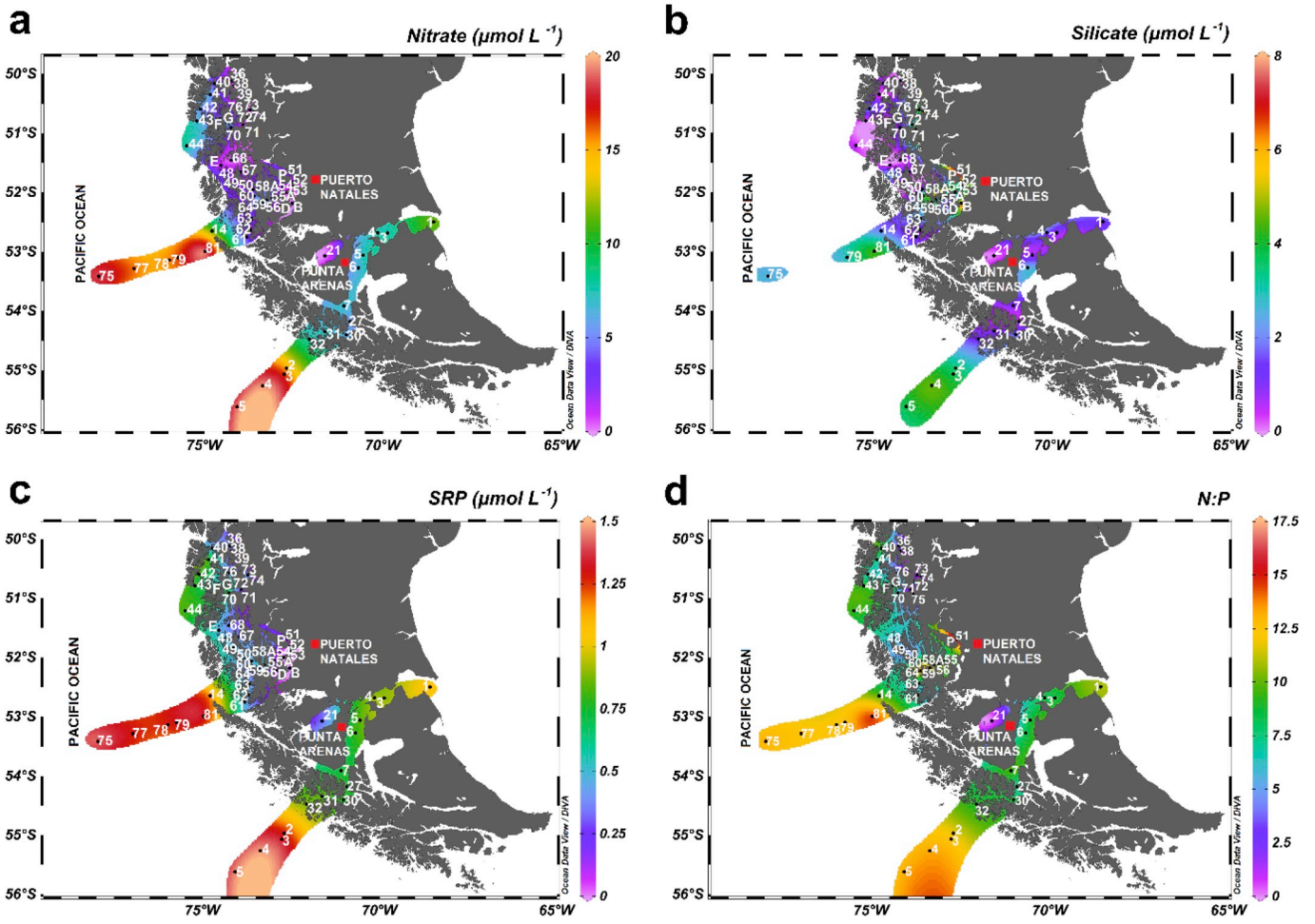

Fig. 5. Surface spatial distribution of **(a)** nitrate, **(b)** SRP, **(c)** silicate and **(d)** N:P relationship in the Magellanic region. Small dots indicate station. Ocean Data View gridding was applied.

Brunswick Peninsula (Pisano, 1973, 1983). It is widely recognized that the majority of global CH_4 production and emissions come from wetlands and flooded ecosystems (Dunfield et al., 1993; Riley et al., 2011; Kirschke et al., 2013).

Surface nutrient distributions are shown in Fig. 5. Similar distributions have previously been reported by Valdenegro and Silva (2003) during the Cimar 3 cruise. Surface NO_3^- varied between 0.05 and 19 µM (mean ± SD values of 5.62 ± 5.57), with the lowest concentrations in the surface layer of fjord heads and channels (potentially undetectable), which gradually increased toward the Inner Sea, with

Table 1
Average and standard deviation of N2O and CH4 concentrations in surface waters, considering 1 and 10 m depth, and estimated air-sea gas fluxes in the Magellanic region.

Geographic place	St.	N_2O (nM) $\bar{X} \pm SD$	CH_4 (nM) $\bar{X} \pm SD$	N_2O flux (μmol m^{-2} d^{-1})	CH_4 flux (μmol m^{-2} d^{-1})
Europa S.	36	11.9 ± 5.7	5.10 ± 1.6	−15.22	4.23
Europa S.	38	12.7 ± 1.0	6.25 ± 6.0	−0.23	−1.45
Europa S.	39	11.9 ± 0.8	–	−0.81	–
Concepción C.	40	13.6 ± 1.1	3.88 ± 3.1	0.69	−0.85
Concepción C.	41	16.5 ± 0.42	6.58 ± 1.7	7.70	9.75
Concepción C.	42	17.0 ± 0.02	5.59 ± 2.1	6.41	5.73
Concepción C.	43*	15.6 ± 1.0	6.22 ± 3.8	4.39	−2.43
Oceanic area	44	13.8 ± 0.7	2.11 ± 0.05	11.10	−3.40
Sarmiento C.	70	16.5 ± 0.3	10.4 ± 3.5	12.53	15.35
Estero Peel	71	13.1 ± 0.2	3.08 ± 3.5	0.19	0.01
Estero Peel	72	13.5 ± 0.4	4.81 ± 0.7	0.11	0,06
Estero Peel	73	13.5 ± 0.5	9.26 ± 7.4	2.01	2.19
Estero Calvo	74	13.9 ± 0.8	6.37 ± 1.8	0.04	0.83
Estero Amalia	75*	14.2 ± 1.7	–	−0.08	–
Sarmiento C.	G	13.1 ± 0.1	2.81 ± 0.7	2.07	0.62
Inocentes C.	F	12.8 ± 0.2	7.15	2.50	−2.17
Smyth C.	50	15.1 ± 0.3	1.84 ± 0.5	1.07	−0.53
Última Esperanza S.	51	13.6 ± 0.1	4.26 ± 0,3	1.97	3.74
Última Esperanza S.	52	13.7 ± 0.07	2.61 ± 0.6	2.09	−0.84
Última Esperanza S.	53	12.1 ± 1.1	4.62 ± 0.5	−3,70	3.95
Almirante Montt G.	P*	21.0 ± 5.7	2.49 ± 0.4	15.6	−2.59
Última Esperanza S.	54	18.1 ± 0.1	3.30 ± 0.5	10.4	1.17
Kirke C.	55	13.3 ± 0.1	3.25 ± 0.3	0.12	0.09
Kirke C.	56	15.4 ± 0.4	4.04 ± 0.1	8.19	3.20
Estero las Montañas	58A	9.69 ± 1.6	13.2 ± 0.2	−2.95	19.90
Union C.	59	16.7 ± 0.8	13.3 ± 0.1	22.1	84.37
Union S.	60	14.8 ± 0.8	13.3 ± 0.05	2.86	26.27
Smyth C.	61	–	12.7 ± 0.5	–	64.01
Smyth C.	62*	16.0 ± 0.5	–	11.2	–
Smyth C.	63	14.6 ± 0.3	13.5 ± 1.1	3.30	15.60
Smyth C.	64	14.3 ± 0.4	12.4 ± 0.09	6.84	59.84
Western Magellan Strait	14	15.71	–	143	–
Eastern Magellan Strait	1	16.4	8.51	36.3	
San Gregorio cape	4	12.07	–	24.8	–
Sector Punta Arenas	6	–	14.45	–	43.61
Sector San Isidro	7	–	7.61	–	2.76
Otway center S.	21	11.4	9.48	35.5	19.55
Magdalena north C.	27	11.4	9.10	−0.22	9.08
Magdalena south C.	30	–	1.81	–	−10.92
Chasco S.	31	16.01	2.56	6.81	−0.68
Cockburn west C.	32	14.47	1.81	6.18	−3.15

(S = Sound; C = Channel; G = Gulf).

values of approximately 15 μM. In the surface water of the open sea, NO_3^- values exceeded 20 μM (typical levels for SAAW) (Fig. 5a). Surface SRP varied between undetectable to 1.48 μM (mean ± SD values of 0.60 ± 0.42), and followed a similar spatial distribution as described for NO_3^- (Fig. 5b). $Si(OH)_4$ varied between undetectable and 7.8 μM, from open ocean to the fjord head, with some peaks observed in the Ultima Esperanza Sound apparently associated with discharge from the Serrano River (Fig. 5c). $Si(OH)_4$ concentration was substantially lower in this region compared to the Inner Sea of northern and central Patagonia (Iriarte et al., 2012; Torres et al., 2014; Yevenes et al., 2017), likely to be due to lower discharge of rivers and the mixing of oceanic water with reduced $Si(OH)_4$ content. In southern Patagonia, there is a lower river discharge in comparison to northern and Central Patagonia, where important rivers, such as the Baker, Pascual, Cisnes Rivers (mean caudal of up to 875 $m^3 s^{-1}$) are present (Dussaillant et al., 2012). Coincidentally, in the Southern Ocean, comparatively low $Si(OH)_4$ concentrations (< 5 μM) were observed to the north of the Polar front in contrast to the south (25–70 μM) (Coale et al., 2004). This $Si(OH)_4$ depletion is characteristic of SAAW, widely documented to be high-nutrient, low-chlorophyll (HNLC) region, particularly during periods of deep vertical mixing (austral winter-spring) (Sarmiento et al., 2004). These results agree with those found by Torres et al. (2014), reporting that $Si(OH)_4$ is negatively correlated with salinity over the entire Patagonia region, given the mixing of high NO_3^- and low $Si(OH)_4$ in SAAW, with high $Si(OH)_4$ and low NO_3^- continental freshwater runoff. In addition, this relationship became weaker from northern to southern Patagonia due to reduced $Si(OH)_4$ inputs from rivers in southern Patagonia. The intensification of a southward $Si(OH)_4$ deficit may be a factor involved in the reported southward reductions in plankton biomass, and an increased occurrence of non-diatom blooms in the southern Patagonia inner sea (Torres et al., 2014). Finally, results showed a wide variation of dissolved inorganic N:P ratios (Fig. 5d), in the open ocean the N:P ratio most similar to the Redfield proportion was observed, however in the inland sea, N:P ratios of around ~12 were observed, indicating a nitrogen deficiency. A very low N:P ratio was observed within the Otway Sound (data not included); relatively high levels of P respect to N from seabird excrements was likely to be similar to other areas with seabird colonies in the sub-Antarctic region (Otero et al., 2018), indicating a rapid mineralization of N with respect to P (Otero et al., 2018), as well as the rapid volatilization of ammonia (Riddick et al., 2012).

3.3. Processes controlling N_2O and CH_4 content and their air-sea fluxes

Table 1 present mean ± SD values of gas concentrations measured at 1 and 10 m depth and N_2O and CH_4 air-sea fluxes based on surface

Table 2
Spearman rank correlation (rs) among physical-chemical variables taken at 1 and 10 m depth in Southern Patagonia Andes and Southern Patagonian Tableland.

Southern Patagonia Andes	Sal	O_2	N_2O	CH_4	SRP	NO_3^-	$Si(OH)_4$
T °C	*0.89*	0.12	0.28	−0.21	*0.60*	*0.66*	−0.31
Sal		0.14	***0.41***	−0.15	***0.73***	***0.77***	−0.24
O_2			0.13	−0.20	0.17	0.11	0.03
N_2O				*0.53*	***0.45***	0.30	0.14
CH_4					0.01	−0.83	0.31
PO_4^{-3}						***0.91***	−0.24
NO_3^-							*−0.36*
Southern Patagonia Tableland	**Sal**	**O_2**	**N_2O**	**CH_4**	**SRP**	**NO_3^-**	**$Si(OH)_4$**
T °C	0.164	0.03	*0.14*	−0.37	0.07	0.01	0.10
Sal		***−0.60***	−0.22	0.14	***0.85***	***0.68***	−0.27
O_2			0.07	***−0.41***	***−0.71***	***−0.71***	−0.02
N_2O				*−0.33*	*−0.32*	−0.14	0.25
CH_4					*0.34*	*0.42*	0.26
PO_4^{-3}						***0.89***	−0.01
NO_3^-							*0.25*

Italics and bold numbers refer to significance values.

(1 m depth) gas concentrations. The estimation of gas fluxes based on Nightingale's parameterization ranged from −15.22 to 36.26 and −10.92–84.36 μmol m^{-2} d^{-1}, for N_2O and CH_4 respectively, but when the estimate is made based on Liss and Merlivat (1986)with 3.6 < U < 13 m·s^{-1} N_2O fluxes fluctuated from −10.78 to 25.99, reducing in 34% respect to Nightingale's parameterization. Similar percentage of reduction was observed for CH_4.

Average regional fluxes for N_2O and CH_4 were 6.20 ± 10.13 and 16.88 ± 27.04 μmol m^{-2} d^{-1}, respectively, indicating that the Magellan Sub-Antarctic region acts as a modest net source of these gases during winter-spring time, although there are great variations, where N_2O and CH_4 undersaturated levels as low 65.3 and 57.4%, respectively, were found in some heads of fjords with glacial influence (Fig. 3); whereas high levels of CH_4 saturation up to 483% were found in waters directly influenced by continental inputs, as observed close to the Minas River (close Punta Arenas city; Fig. 4). Significantly greater CH_4 effluxes were estimated in sampled stations in the Strait of Magellan Strait (sampled during Cimar 16 cruise) compared to more northern fjord stations (sampled during Cimar 15 cruise).

A spatially comparison of the two regions indicated, the mean flux of CH_4 in Magellanic region was one order of magnitude higher than the values estimated for the open ocean (~0.4 μmol m^{-2} d^{-1}) (Bates et al., 1996), and slightly lower than the standard values observed on the continental shelves (~30 μmol m^{-2} d^{-1}). However, in other fjords the CH_4 fluxes ranged from 10 to 100 μmol m^{-2} d^{-1} (Borges et al., 2016), the extend of the variation is dependent on the intensity of eutrophication, changes in land use, and geomorphologic characteristics such as depth, as well as the presence of marine seeps. Furthermore, rates of N_2O exchange are similar to the values observed in the open ocean (Nevison et al., 1995), and comparatively low to N_2O fluxes estimated in other coastal areas, even in fjords. These observations are likely to be a result of the input of marine and continental sources with N_2O levels in equilibrium with (or lower than) the atmosphere. In fact, high N_2O levels are estimated for rivers and areas with intense human activity, such as agriculture, mainly due to the use of fertilizers (Seitzinger et al., 2000). In the Magellanic region, there is low human activity and additionally the SAAW has low N_2O levels. Thus, estimated N_2O fluxes are relatively low when are compared with those found in north Patagonia (Yevenes et al., 2017; Farías et al., 2017) and an estuary located in central Chile (Daniel et al., 2013).

Temporally, annual extrapolation is restricted due to the lack of measurements recorded during the summer and fall. This study provides the first N_2O and CH_4 data from samples taken from the water column in the Magellan Sub-Antarctic region; therefore, it is challenging to extrapolate the sink/source status temporally within the region. In order to provide realistic and accurate inputs into predictive models of future climate change scenarios, oceanic inventories of these greenhouse gases needs to be improved, as indicated by the IPCC (2013). The seasonal analysis indicated that there not may expect considerable seasonal changes due to the absence of environmental variations that may cause a considerable increase the nitrifying activity (responsible for N_2O production), and no seasonal changes in river discharge and runoff that could affect temporal variability of N_2O. On the contrary, there may be seasonal changes in air-sea CH_4 fluxes associated primarily with temperature variations; considering that an increase in temperature during the summer favours CH_4 regeneration in soils as a part of the decomposition of organic matter. Indeed, it has been observed that CH_4 production in soil has a greater dependence on temperature (Dunfield et al., 1993). Thus in the austral summer, when atmospheric temperatures are higher, increased microbial CH_4 production in soils is expected.

Table 2 shows the Spearman correlation analysis for environmental variables (temperature, salinity, O_2, SRP, NO_3 -, $Si(OH)_4$, CH_4 and N_2O) in the surface layer. Data was separated into the two areas; those influenced by the southern Andes region (Sts. 71, 75, 70, G, F, 51, 52, 53, 54, 55, 56, 58A, 59, 60, 50), and those associated with the Patagonian tableland (Sts. 1, 3, 4, 5, 6, 7, 21, 27, 30, 31, 32), the latter includes the Magellan Strait. In the Andes range, N_2O was significantly and positively correlated with salinity (rs: 0.44 $p < 0.05$), i.e., N_2O distribution depended on mixing between the warmer and saltier SAAW and the cooler and fresher estuarine waters, rather than a thermal dependence. In addition, significant positive correlations were also found between salinity vs. nutrients (NO_3^-, SRP) (rs = 0.77 and 0.73, respectively, $p < 0.05$), as well as between N_2O and SRP (0.45, $p = 0.05$), reaffirming that the nutrient and N_2O origin was from a marine water mass.

Dissolved CH_4 concentrations and $Si(OH)_4$ did not show any significant correlation with physical variables and other nutrients, reinforcing that riverine contributions and discharges are low in this region (west side); an exception existed in the CH_4 hot spot, observed near the city of Punta Arenas. This pattern was different to that observed in the fjords of northern Patagonia, where river discharge was a source of $Si(OH)_4$ and CH_4 (Farías et al., 2017). In the Patagonia tableland, predominantly in the Magellan Strait, the lack of dependence of CH_4 distribution with physical and nutrient variables suggests the presence of other continental sources, rather than the occurrence of physical processes such as water mass mixing or a more complex mixing circulation.

3.4. Cross section distribution of salinity, nitrous oxide and methane

Fig. 6 illustrates the cross section of physical and chemical variables from the Concepcion Channel (Fig. 6a) and Smyth Channel (Fig. 6b). SAAW flows into the inner sea, towards several channels and sounds, progressively mixing without flowing estuarine water. This generates modified SAAW (Silva et al., 1998), which shows a conservative mixing of salinity (with salinities lower than 14.5 in the fiord heads) and temperature (not shown). Also, NO_3^- and SRP (not shown) presented a semi-conservative behavior due to SAAW being a major nutrient source, as described by Silva et al. (2002).

Conversely, gases presented heterogeneous distributions, particularly CH_4. Indeed, CH_4 did not correlate with temperature and salinity (Table 2), but N_2O showed a more conservative behavior and more uniform distribution in the surface layer. In the cross section along the Concepcion and Smyth channels, N_2O inputs are sourced from more saline water, while brackish water is N_2O depleted. However, is appears

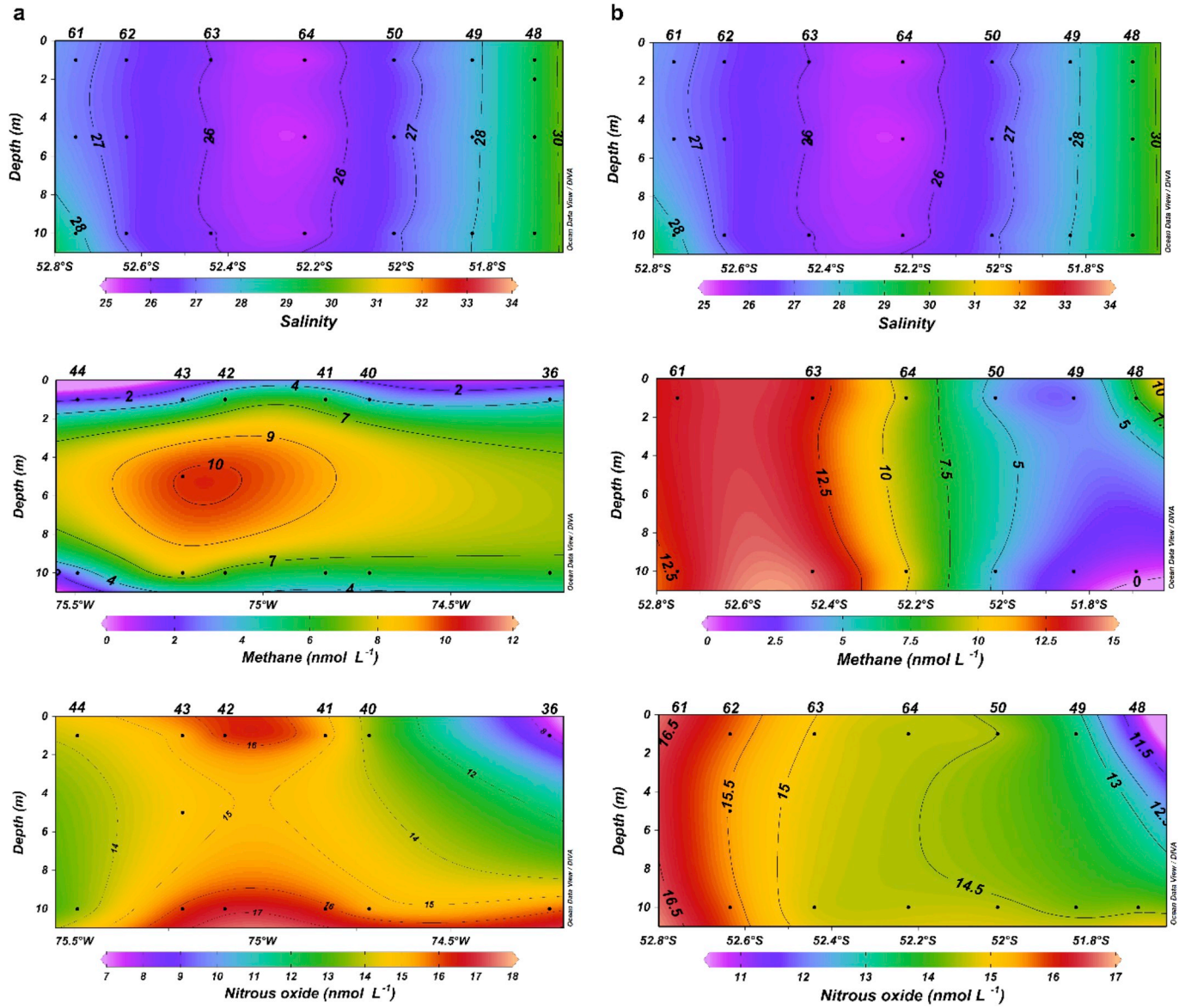

Fig. 6. Cross section distribution of the oceanographic/biogeochemical conditions from two selected transects: **(a)** Concepcion channel and **(b)** Smyth channel.

that local N_2O production in the Inner Sea occurs following the observations from St. 51, St 52. Other previous studies in the fjords in the north of Patagonia have attributed accumulation to nitrification (Yevenes et al., 2017). The cross section of CH_4 from the Concepcion channel presented relatively low gas levels, whereas the western microbasin within the Smyth channel (that connects with the Magellan Strait, Fig. 1) revealed elevated CH_4 accumulation with respect to the inner sea.

3.5. Vertical profiles of gases and physical variables in selected stations

Fig. 7 presents vertical physical-chemical profiles, indicating the differences between a station located in the interior sea (St. 62 and P) to one from the open sea (e.g., St. 43). In offshore waters, vertical distribution of salinity and temperature was less abrupt with respect to profiles in the Inner Sea (Fig. 7a, d, 7g). Indeed, the water column in fjords and channels was characterized by strong salinity and temperature gradients, with the halocline generally occurring above 10 m depth (Fig. 7d and g). Regarding the distribution of dissolved O_2, its concentration decreased from 330 μM at the surface to 272 μM at 100 m depth, i.e., high O_2 conditions were maintained through most of the sampled stations (Fig. 7b and e), except for St. P, located in the Almirante Montt sound, showing anomalous behavior, with the lowest recorded dissolved O_2 concentration of 14 μM (4% saturation) at 150 m (Fig. 7h). Unlike other stations where N_2O distribution was almost homogeneous (Fig. 7b and e), at this station N_2O distribution peaked up to 37.8 nM (312% saturation) at 100 m depth (Fig. 7h), which was the maximum recorded value from the study area.

N_2O accumulation frequently occurs at the upper oxycline, regulated by the oxygen gradient, with partial denitrification and aerobic ammonium oxidation likely to be responsible for N_2O accumulation (Farías et al., 2009; Kock et al., 2016). Recent evidence has indicated that archaeal ammonia-oxidizer (AOA) dominance at the oxycline leads to $_{N2}O$ production as a by-product of nitrification, or via hybrid N_2O formation (Löscher et al., 2012; Trimmer et al., 2016). Subsequently, N_2O (and also NO_3) abruptly decreased to 17.6 nM at 150 m depth, where dissolved O_2 is sufficiently low enough for anaerobic respiration of organic matter via canonical denitrification (Farías et al., 2009). Remarkably, Silva and Vargas (2014) observed that 86 out of the 90 channels in Patagonia fjords were well oxygenated, four are permanently hypoxic (< 88 μM O_2), and none are anoxic. Almirante Montt sound was one of the fjords identified as hypoxic, where ventilation was

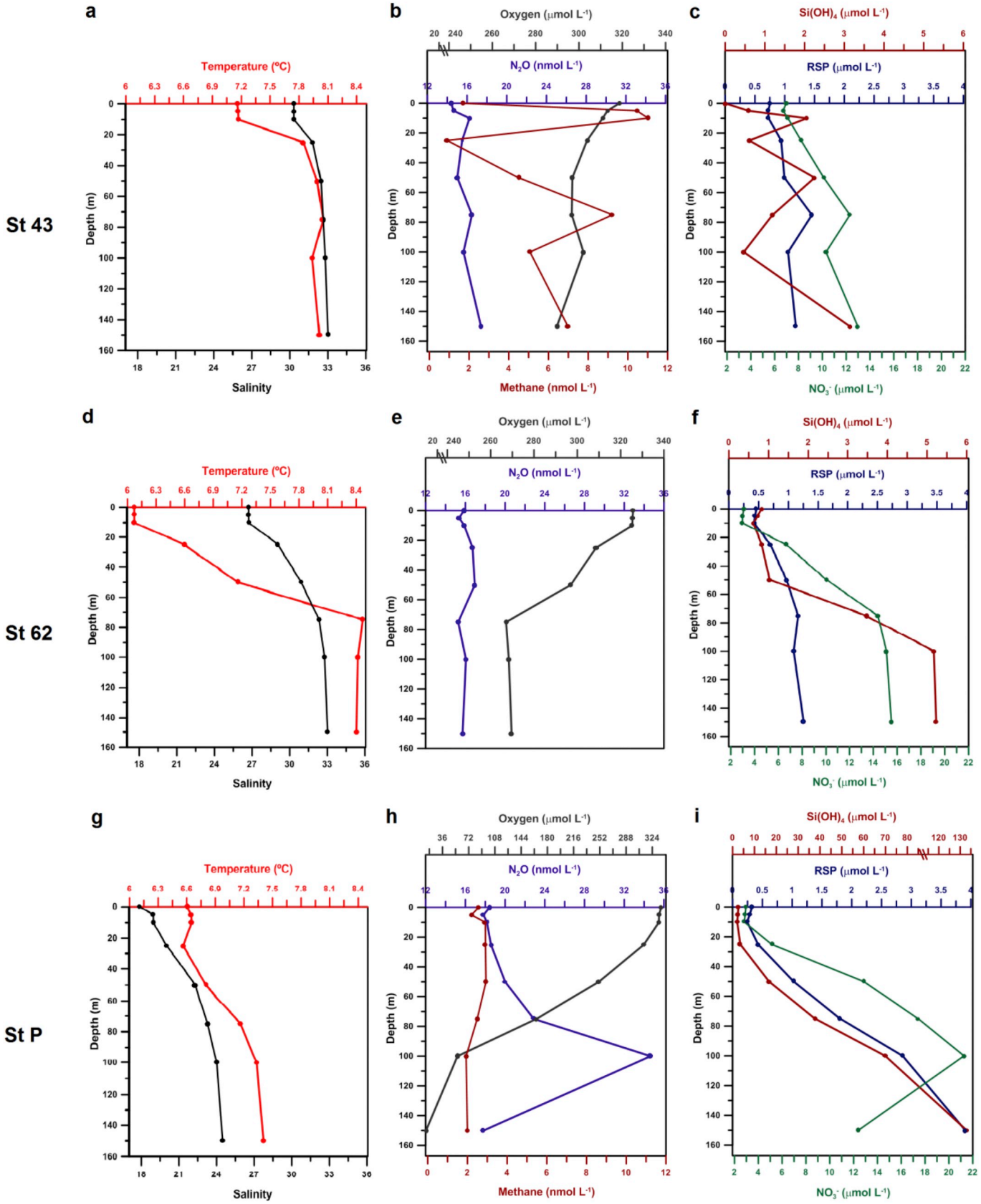

Fig. 7. Vertical distribution of; (a,d,g) temperature and salinity, (b,e,h) dissolved gases as oxygen, methane and nitrous oxide and (c,f,h) nutrients included NO_3^-, SRP and $Si(OH)_4$) at selected stations from marine (St. 43) the fjord (St. 62) and sound (St. P).

predominantly caused by physical processes rather than biogeochemical ones (Silva and Vargas, 2014).

Vertical CH_4 distribution at St. 43 peaked at different depths whereas at St P, CH_4 distributed almost homogenously (Fig. 7b); superficially one of them was located at the pycnocline which is expected due to the accumulation of particles (Karl; Tilbrook, 1994) as it has been observed in fjords of north Patagonia (Farías et al., 2017). The origin of CH_4 in surface water has been debated for long time; today is known that methylotrophic micro-organisms play an important role in generating CH_4 using different organic substrates according to environment (Damm et al., 2010; Karl et al., 2008; Repeta et al., 2016) and being responsible for CH_4 oversaturation in oxygenated waters. Finally, NO_3^- and PO_4^{3-} increased with depth (Fig. 7c and f, except at St P (Fig. 7i), where NO_3^- seems to be used as an electron acceptor during dissimilative NO_3^- reduction according to O_2 distribution. Si $(OH)_4$ peaked at several depth at St 43 (Fig. 7c) with a distribution similar to CH_4,; in the other stations (Fig. 7f and i), $Si(OH)_4$ increased with depth.

4. Conclusion

N_2O profiles are uniform and their concentrations are controlled by the gradual mixing of SAAW, which provides relatively higher concentrations of both N_2O and nutrients. Superficially, the concentration of N_2O varies from undersaturated levels at head of some fjords to slightly supersaturated at station under more marine. The CH_4 profiles are more variable and surface distribution of CH_4 fluctuates from concentration close to the equilibrium in waters under more marine influence to higher CH_4 concentration the Inner Sea (except for some fjords with glacial influence). Average air-sea fluxes of N_2O and CH_4 are 6.21 and 16.88 $\mu mol\, m^{-2}\, d^{-1}$, respectively, indicating that the Magellan Sub-Antarctic region acts as a modest source of these gases to the atmosphere. When these gas emissions are compared with those form other ecosystems, the magnitude of gas exchanges account of systems with little N_2O and CH_4 entry from marine and continental waters and little human intervention except for a couple of stations that account for terrestrial sources or the effect of the penguins. This study will stand as a baseline to register medium and long-term natural and anthropogenic variations, including climate change.

Acknowledgements

This research was funded by National Oceanographic Committee (Comité Oceanográfico Nacional) (CONA) and the Chilean Navy, as part of the multidisciplinary project CIMAR 15 and 16. Support was provided by FONDECYT # 1161138 (Laura Farías) and Comisión Nacional de Investigación Científica y Tecnológica(CONICYT)/FONDAP program no. 1511009 (CR^2). We thank the staff at Silva's lab (PUCV) for their invaluable collaboration during sampling. We also appreciate the critical revision by Josefa Verdugo and Armando Sepulveda-Jaugueri.

Appendix A. Supplementary data

Supplementary data to this article can be found online at https://doi.org/10.1016/j.ecss.2018.10.020.

References

Araya-Vergara, J.F., 2004. Chile. In: Bird, E.C.F. (Ed.), The World's Coasts: Online. Springer Reference, New York, pp. 1–24. http://www.springer.com/geosciences/oceanog.raphy/book/978-0-306-48369-1, Accessed date: 18 November 2017.

Atlas, E., Hager, S., Gordon, L., Park, P., 1971. A practical manual for use of the Technicon Autoanalyzer in sea water nutrient analyses. O.S.U., Dept. Oceanogr. Tech. rep. 215.

Bange, H.W., Bartell, U.H., Rapsomanikis, S., Andreae, M.O., 1994. Methane in the Baltic and North Seas and a reassessment of the marine emissions of methane. Global Biogeochem. Cycles 8, 465–480.

Bange, H., Freing, W.A., Kock, A., Löscher, C.R., 2010. Marine pathways to nitrous oxide. In: Smith, K. (Ed.), Nitrous Oxide and Climate Change. Earthscan, London, UK, pp. 36–62.

Bates, T.S., Kelly, K.C., Johnson, J.E., Gammon, R.H., 1996. A reevaluation of the open ocean source of methane to the atmosphere. J. Geophys. Res. Atmospheres 101 (D3), 6953–6961. https://doi.org/10.1029/95JD03348.

Borges, A.V., Abril, G., 2011. Carbon dioxide and methane dynamics in estuaries. In: In: Wolanski, E., McLusky, D.S. (Eds.), Treatise on Estuarine and Coastal Science, vol. 5. Waltham Academic Press, pp. 119–161.

Borges, A.V., Champenois, W., Gypens, N., Delille, B., Harlay, J., 2016. Massive marine methane emissions from near-shore shallow coastal areas. Sci. Rep. 6, 27908. https://doi.org/10.1038/srep27908.

Bouman, H.A., Lepèrec, C., Scanlan, D.J., Ulloa, O., 2012. Phytoplankton community structure in a high-nutrient, low-chlorophyll region of the eastern Pacific Subantarctic region during winter-mixed and summer-stratified conditions. Deep-Sea Res. 69, 1–11.

Buschmann, A., López, D., Medina, A., 1996. A review of the environmental effects and alternative production strategies of marine aquaculture in Chile. Aquacult. Eng. 15 (6), 397–421.

Cáceres, M., Valle-Levinson, A., Atkinson, L., 2003. Observations of cross-channel structure of flow in an energetic tidal channel. J. Geophys. Res. Oceans 108 (C4), 3114.

Cameron, W.H., Pritchard, D.W., 1963. Estuaries. In: Hill, M.N. (Ed.), The Sea. Wiley, New York, pp. 306–324.

Carini, P., White, A.E., Campbell, E.O., Giovannoni, S.J., 2014. Methane production by phosphate-starved SAR11 chemoheterotrophic marine bacteria. Nat. Commun. 5, 4346. https://doi.org/10.1038/ncomms5346.

Carrasco, C., Karstensen, J., Farías, L., 2017. On the nitrous oxide accumulation in intermediate waters of the eastern south Pacific Ocean. Front. Mar. Sci. 4, 24. https://doi.org/10.3389/fmars.2017.00024.

Casassa, G., Rivera, A., Aniya, M., Naruse, R., 2002. Current knowledge of the southern Patagonia ice Fields. In: Casassa, G.F., Sepúlveda, V., Sinclair, R. (Eds.), The Patagonian Ice Fields: a Unique Natural Laboratory for Environmental and Climate Change Studies. Kluwer Academic, New York, pp. 67–83.

Ciais, P., Sabine, C., Bala, G., Bopp, L., Brovkin, V., Canadell, J., Chhabra, A., DeFries, R., Galloway, J., Heimann, M., Jones, C., Le Quéré, C., Myneni, R.B., Piao, S., Thornton, P., 2013. Carbon and other biogeochemical cycles. In: Stocker, T.F., Qin, D., Plattner, G.-K., Tignor, M., Allen, S.K., Boschung, J., Nauels, A., Xia, Y., Bex, V., Midgley, P.M. (Eds.), Climate Change 2013: the Physical Science Basis. Contribution of Working Group I to the Fifth Assessment Report of the Intergovernmental Panel on Climate Change. Cambridge University Press, Cambridge, United Kingdom and New York, NY, USA, pp. 465–489. https://www.ipcc.ch/pdf/assessment-report/ar5/wg1/WG1AR5_Chapter06_FINAL.pdf, Accessed date: 15 October 2018.

Coale, K.H., Johnson, K.S., Chavez, F.P., Buesseler, K.O., Barber, R.T., Brzezinski, M.A., 2004. Southern Ocean iron enrichment experiment: carbon cycling in high- and low-Si waters. Science 304, 408–414.

Coronato, A., Coronato, F., Mazzoni, E., Vázquez, M., 2008. The physical geography of Patagonia and Tierra del Fuego. In: Rabassa, J. (Ed.), The Late Cenozoic of Patagonia and Tierra del Fuego. Elsevier, Amsterdand, pp. 13–56.

Damm, E., Helmke, E., Thoms, S., Schauer, U., Nöthing, E., Bakker, K., Kiene, R.P., 2010. Methane production in aerobic oligotrophic surface water in the central Artic Ocean. Biogeosciences 7, 1099–1108.

Damm, E., Rudels, B., Schauer, U., Mau, S., Dieckmann, G., 2015. Methane excess in Arctic surface water-triggered by sea ice formation and melting. Science Report 5, 16179. https://doi.org/10.1038/srep16179.

Daniel, I., De Grandpre, M., Farías, L., 2013. Greenhouse gas emissions from Tubul-Raqui estuary (central Chile 36ºS). Estuar. Coast Shelf Sci. 134, 31–44. https://doi.org/10.1016/j.ecss.2013.09.019.

Denman, K.L., Brasseur, G., Chidthaisong, A., Ciais, P., Cox, P.M., Dickinson, R.E., Hauglustaine, D., Heinze, C., Holland, E., Jacob, D., Lohmann, U., Ramachandran, S., da Silva Dias, P.L., Wofsy, S.C., Zhang, X., 2007. Couplings between changes in the climate system and biogeochemistry. In: Solomon, S., Qin, D., Manning, M., Chen, Z., Marquis, M., Averyt, K.B., Tignor, M., Miller, H.L. (Eds.), Climate Change. 2007. The Physical Science Basis. Contribution of Working Group I to the Fourth Assessment Report of the Intergovernmental Panel on Climate Change (IPCC). Cambridge University Press, Cambridge. United Kingdom and New York. USA, pp. 499–587. http://www.ipcc.ch/pdf/assessmentreport/ar4/wg1/ar4-wg1-chapter7.pdf, Accessed date: 15 October 2018.

DGA, 2012. Diagnóstico y clasificación de los cursos y cuerpos de agua según objetivos de calidad. Preparado por Cade-Idepe. Consultores en Ingeniería para el Ministerio de Obras Públicas. Dirección Gral. Aguas, pp. 89.

Dussaillant, A., Buytaert, W., Meier, C., Espinoza, F., 2012. Hydrological regime of remote catchments with extreme gradients under accelerated change: the Baker basin in Patagonia. Hydrol. Sci. J. 57, 1530–1542. https://doi.org/10.1080/02626667.2012.726993.

Dunfield, P., Knowles, R., Dumont, R., Moore, T.R., 1993. Methane production and consumption in temperate and subarctic peat soils: response to temperature and pH. Soil Biol. Biochem. 25, 321–326. https://doi.org/10.1016/0038-0717(93)90130-4.

Farías, L., Castro-González, M., Cornejo, M., Charpentier, J., Faúndez, J., Boontanon, N., Yoshida, N., 2009. Denitrification and nitrous oxide cycling within the upper oxycline of the oxygen minimum zone off the eastern tropical South Pacific. Limnol. Oceanogr. 54, 132–144.

Farías, L., Florez-Leiva, L., Besoain, V., Fernandez, C., 2015. Dissolved greenhouse gases (nitrous oxide and methane) associated with the natural iron- fertilized Kerguelen region (KEOPS 2 cruise) in the Southern Ocean. Biogeosciences 12, 1925–1940. https://doi.org/10.5194/bgd-11-12531-2014.

Farías, L., Sanzana, K., Sanhueza-Guevara, S., Yevenes, M., 2017. Dissolved methane distribution in the Reloncaví Fjord and adjacent marine system during austral winter (41°-43° S). Estuar. Coast 40, 1592–1606.

Fyfe, J.C., Saenko, O.A., Zickfeld, K., Eby, M., Weaver, A.J., 2007. The role of poleward intensifying winds on Southern Ocean warming. J. Clim. 20, 5391–5400.

Garratt, J.R., 1977. Review of drag coefficients over oceans and continents. Mon. Weather

Rev. 150, 915–929.
Gille, S.T., 2002. Warming of the Southern Ocean since the 1950's. Science 295, 1275–1277.
Grasshoff, K., Ehrhardt, M., Kremling, K., 1983. Methods of Sea Water Analysis. Verlag Chemie Int. Weinheim, pp. 197.
Hartin, C.A., Fine, R.A., Sloyan, B.M., Talley, L.D., Chereskin, T.K., Happell, J., 2011. Formation rates of subantarctic mode water and antarctic intermediate water within the south pacific. Deep-Sea Res. I 58, 524–534.
Holmes, M.E., Sansone, F.J., Rust, T.J., Popp, N., 2000. Methane production, consumption, and air-sea exchange in the open ocean: an evaluation based on carbon isotopic ratios. Global Biogeochem. Cycles 14, 1–10.
Holte, J.W., Talley, L.D., Chereskin, T.K., Sloyan, B.M., 2012. The role of air-sea fluxes in Subantarctic Mode Water formation. J. Geophys. Res. 117, 3–40. https://doi.org/10.1029/2011JC007798.
IPCC, 2013. Climate change. The physical science basis. In: Contribution of Working Group, I to the Fourth Assessment Report of the Intergovernmental Panel on Climate Change. Cambridge University Press, Cambridge, UK and New York, USA, pp. 996.
Iriarte, J.L., Pantoja, S., González, H.E., Silva, G., Paves, H., Labbé, P., Rebolledo, L., Van Ardelan, M., Häusserman, V., 2012. Assessing the micro-phytoplankton response to nitrate in Comau Fjord (42°S) in Patagonia (Chile), using a microcosms approach. Environ. Monit. Assess. 185, 55–70.
Iriarte, J., León-Muñoz, J., Marcé, R., Clément, A., Lara, C., 2016. Influence of seasonal freshwater streamflow regimes on phytoplankton blooms in a Patagonian fjord. New Zeal J. Mar. Fresh. 8330, 1–12.
Karl, D.M., Tilbrook, B.D., 1994. Production and transport of methane in oceanic particulate matter. Nature 368, 732–734.
Karl, D., Beversdorf, L., Björkman, K.M., Church, M.J., Martinez, A., DeLong, E.F., 2008. Aerobic production of methane in the sea. Nat. Geosci. 1, 473–478.
Karstensen, J., Quadfasel, D., 2002. Formation of southern hemisphere thermocline waters: water mass conversion and subduction. J. Phys. Oceanogr. 32, 3020–3038.
Kirschke, S., Bousquet, P., Ciais, P., Saunois, M., Canadell, J.G., Dlugokencky, E.J., Bergamaschi, P., Bergmann, D., Blake, D.R., Bruhwiler, L., Cameron-Smith, P., Castaldi, S., Chevallier, F., Feng, L., Fraser, A., Heimann, M., Hodson, E.L., Houweling, S., Josse, B., Fraser, P.J., Krummel, P.B., Lamarque, J.F., Langenfelds, R.L., Le Quéré, C., Naik, V., O'Doherty, S., Palmer, P.I., Pison, I., Plummer, D., Poulter, B., Prinn, R.G., Rigby, M., Ringeval, B., Santini, M., Schmidt, M., Shindell, D.T., Simpson, I.J., Spahni, R., Steele, L.P., Strode, S.A., Sudo, K., Szopa, S., van der Werf, G.R., Voulgarakis, A., van Weele, M., Weiss, R.F., Williams, J.E., Zeng, G., 2013. Three decades of global methane sources and sinks. Nat. Geosci. 6, 813–823. https://doi.org/10.1038/ngeo1955.
Kitidis, V., Upstill-Goddard, R.C., Anderson, L.G., 2010. Methane and nitrous oxide in surface water along the north-west passage, arctic ocean. Mar. Chem. 121, 80–86.
Kock, A., Arévalo-Martínez, D.L., Löscher, C.R., Bange, H.W., 2016. Extreme nitrous oxide accumulation in the coastal oxygen minimum zone off Peru. Biogeosciences 13, 827–840.
Liss, P.S., Merlivat, L., 1986. Air-sea gas exchange rates: introduction and synthesis. In: Buat-Menard, P. (Ed.), The Role of Air-sea Exchange in Geochemical Cycling. Reidel, Boston, pp. 113–129.
Llanillo, P.J., Karstensen, J., Pelegrí, J.L., Stramma, L., 2013. Physical and biogeochemical forcing of oxygen and nitrate changes during El Niño/El Viejo and La Niña/La Vieja upper-ocean phases in the tropical eastern South Pacific along 86°W. Biogeosciences 10, 6339–6355. https://doi.org/10.5194/bg-10-6339-2013.
Löscher, C.R., Kock, A., Könneke, M., LaRoche, J., Bange, H.W., Schmitz, R.A., 2012. Production of oceanic nitrous oxide by ammonia-oxidizing archaea. Biogeosciences 9, 2419–2429.
McAulliffe, C., 1971. Gas chromatographic determination of solutes by multiple phase equilibrium. Chem. Technol. 1, 46–51.
Naruse, R., Aniya, M., 1992. Outline of glacier research project in Patagonia. 1990. Bull. Glacier Res. 10, 31–38.
Nevison, C.D., Weiss, R.F., Erickson, D.J., 1995. Global oceanic emissions of nitrous oxide. J. Geophys. Res. 100, 15809–15820. https://doi.org/10.1029/95JC00684.
Nevison, C.D., Lueker, T.J., Weiss, R.F., 2004. Quantifying the nitrous oxide source from coastal upwelling. Global Biogeochem. Cycles 18, GB1018. https://doi.org/10.1029/2003GB002110.
Niemeyer, H., Cereceda, P., 1984. Hidrografía. Geografía de Chile. Tomo VIII. Instituto. geográfico militar. Chile.
Nightingale, P.D., Malin, G., Law, C.S., Watson, A.J., Liss, P.S., Liddicoat, M.I., Boutin, J., Upstill-Goddard, R.C., 2000. *In-situ* evaluation of air-sea gas exchange parameterizations using novel conservative and volatile tracers. Global Biogeochem. Cycles 14, 373–387.
Oke, P.R., England, M.H., 2004. Oceanic response to changes in the latitude of the Southern Hemisphere subpolar westerly winds. J. Clim. 17, 1040–1054.
Otero, X.J., De La Peña-Lastra, S., Pérez-Alberti, A., Osorio Ferreira, T., Huerta-Diaz, M.A., 2018. Seabird colonies as important global drivers in the nitrogen and phosphorus cycles. Nat. Commun. 9, 246. https://doi.org/10.1038/s41467-017-02446-8.
Pantoja, S., Iriarte, L.J., Daneri, G., 2011. Oceanography of the chilean Patagonia. Continent. Shelf Res. 31, 149–153.
Pisano, V.E., Dimitri, M.J., 1973. Estudio ecológico de la región continental sur del área Andino-Patagónica. I. Contribución a la fitogeógrafía de comunidades arbóreas, arborescentes y herbáceas al sur-este del ventisquero Moreno, Parque Nacional "Los Glaciares", Santa Cruz, Argentina. Ans. Inst. Pat. 4, 207–272 Punta Arenas. Chile.
Pisano, E., 1983. The magellanic tundra complex. In: Gore, A.J.P. (Ed.), Mires: Swamp, Bog, Fen and Moor. B. Regional Studies. Elsevier Science Publisher of Scientific, Amsterdam, The Netherlands, pp. 295–329.
Portmann, R.W., Daniel, J.S., Ravishankara, A.R., 2012. Stratospheric ozone depletion due to nitrous oxide: influences of other gases. Philos. Trans. R. Soc. 367, 1256–1264. https://doi.org/10.1098/rstb.2011.0377.
Randall, K., Scarratt, M., Levasseur, M., Michaud, S., Xie, H., Gosselin, M., 2012. First measurements of nitrous oxide in Arctic sea ice. J. Geophys. Res. Oceans 117, C00G15. https://doi.org/10.1029/2011JC007340.
Repeta, D.J., Ferrón, S., Sosa, O.A., Johnson, C.G., Repeta, L.D., Acker, M., DeLong, E., Karl, D.M., 2016. Marine methane paradox explained by bacterial degradation of dissolved organic matter. Nat. Geosci. 9 (12), 884.
Riley, W.J., Subin, Z.M., Lawrence, D.M., Swenson, S.C., Torn, M.S., 2011. Barriers to predicting changes in global terrestrial methane fluxes: analyses using CLM4Me, a methane biogeochemistry model integrated in CESM. Biogeosciences 8, 1925–1953.
Reeburgh, W.S., 2007. Oceanic methane biogeochemistry. Chem. Rev. 107, 486–513.
Rhee, T.S., Kettle, A.J., Andreae, M.O., 2009. Methane and nitrous oxide emissions from the ocean: a reassessment using basin-wide observations in the Atlantic. J. Geophys. Res. 114, D12304. https://doi.org/10.1029/2008JD011662.
Riddick, S.N., Dragosits, U., Blackall, T.D., Daunt, F., Wanless, S., Sutton, M.A., 2012. The global distribution of ammonia emissions from seabird colonies. Atmos. Environ. 55, 319–327.
Sarmiento, J.L., Gruber, N., Brzezinski, M.A., Dunne, J.P., 2004. High-latitude controls of thermocline nutrients and low latitude biological productivity. Nature 427 (6969), 56–60.
Saunois, M., Jackson, R.B., Bousquet, P., Poulter, B., Canadell, J.G., 2016. The growing role of methane in anthropogenic climate change. Environ. Res. Lett. 11, 120–207. https://doi.org/10.1088/1748-9326/11/12/120207.
Schwander, J.B., Stauffer Sigg, A., 2017. Air mixing in firn and the age of the air at pore close-off. Ann. Glaciol. 10, 141–145. https://doi.org/10.1017/S0260305500004328.
Seitzinger, S.P., Kroeze, C., Styles, R.V., 2000. Global distribution of N2O emission from system: natural emissions and anthropogenic effects. Chemosphere Global Change Sci. 2, 267–279.
Sievers, H., Silva, N., 2008. Water masses and circulation in austral Chilean channels and fjords. In: Silva, N., Palma, S. (Eds.), Progress in the Oceanographic Knowledge of Chilean Interior Water from Puerto Montt to Cape Horn. Comité Oceanográfico Nacional. Pontificia Universidad Católica de Valparaíso, Valparaíso, pp. 53–58.
Silva, N., Calvete, C., Sievers, H.A., 1998. Masas de agua y circulación general para algunos canales australes chilenos entre Puerto Montt y laguna San Rafael (Crucero CIMAR-Fiordo 1). Cienc. Tecnol. Mar 21, 17–48.
Silva, N., Calvete, C., 2002. Características oceanográficas físicas y químicas de canales australes chilenos entre el golfo de Penas y el estrecho de Magallanes (Crucero CIMAR 2 Fiordos). Cienc. Tecnol. Mar 25, 23–88.
Silva, N., Vargas, C.A., 2014. Hypoxia in chilean patagonian fjords. Prog. Oceanogr. 129, 62–74.
Sun, L.G., Zhu, R.B., Xie, Z.Q., Xing, G.X., 2002. Emissions of nitrous oxide and methane from Antarctic tundra: role of penguin dropping deposition. Atmos. Environ. 36, 4977–4982.
Suntharalingam, P., Sarmiento, J.L., 2000. Factors governing the oceanic nitrous oxide distribution: simulations with an ocean general circulation model. Global Biogeochem. Cycles 14, 429–454. https://doi.org/10.1029/1999GB900032.
Thompson, D.W.J., Solomon, S., 2002. Interpretation of recent Southern Hemisphere climate change. Science 296, 895–899.
Trimmer, M., Chronopoulou, P.-M., Maanoja, S.T., Upstill-Goddard, R.C., Kitidis, V., Purdy, K.J., 2016. Nitrous oxide as a function of oxygen and archaeal gene abundance in the North Pacific. Nat. Commun. 7, 13451.
Torres, R., Nelson, S., Brian, R., Máximo, F., 2014. Silicic acid enrichment of subantarctic surface water from continental inputs along the Patagonian archipelago interior sea (41–56° S). Prog. Oceanogr. 129, 50–61.
Tsuchiya, M., Talley, L.D., 1998. A Pacific hydrographic section at 88°W: water-property distribution. J. Geophys. Res. 103 12,898–12,918.
US EPA. United Stated Enviromental Protection, 2010. Methane and Nitrous Oxide Emission from Natural Sources. Washington, DC. pp. 194.
Valdenegro, A., Silva, N., 2003. Caracterización oceanográfica física y química de la zona de canales y fiordos australes de Chile entre el estrecho de Magallanes y cabo de Hornos (CIMAR 3 Fiordos). Cienc. Tecnol. Mar. 26, 19–60.
Valle-Levinson, A., Sarkar, N., Sanay, R., Soto, D., León, J., 2007. Spatial structure of hydrography and flow in a Chilean fjord. Estuario Reloncaví. Estuar. Coasts 30, 113–126.
Vargas, C., Cuevas, A., Silva, N., González, H.E., De Pol-Holz, R., Narváez, D.A., 2018. Influence of glacier melting and river discharges on the nutrient distribution and DIC recycling in the southern chilean Patagonia. J. Geophys. Res. *Biogeoscience* 123, 256–270. https://doi.org/10.1002/2017JG003907.
Verdugo, J., Damm, E., Snoeijs, P., Díez, B., Farías, L., 2016. Climate relevant trace gases (N_2O and CH_4) in the eurasian basin (arctic ocean). Deep-Sea Res. I 117, 84–94.
Wanninkhof, R., 2014. Relationship between wind speed and gas exchange over the ocean revisited. Limnol Oceanogr. Methods 12, 351–362.
Weiss, R.F., Price, B.A., 1980. Nitrous oxide solubility in water and seawater. Mar. Chem. 8, 347–359.
Wiesenburg, D.A., Guinasso Jr., N.L., 1979. Equilibrium solubilities of methane, carbon monoxide, and hydrogen in water and sea water. J. Chem. Eng. Data 24, 356–360.
Williams, J., Crutzen, P.J., 2010. Nitrous oxide from aquaculture. Sciences 3, 143–145.
Willis, M.J., Melkonian, A.K., Pritchard, M.E., Ramage, J.M., 2012. Ice loss rates at the Northern Patagonian Ice Field derived using a decade of satellite remote sensing. Remote Sens. Environ. 117, 184–198.
Yevenes, M.A., Bello, E., Sanhueza-Guevara, S., Farías, L., 2017. Spatial distribution of nitrous oxide (N_2O) in the reloncaví estuary–sound and adjacent sea (41°–43°S), chilean Patagonia. Estuar. Coast 40, 807–821.
Zamora, M.E., Santana, A.A., 1979. Características climáticas de la costa Occidental de la Patagonia entre las latitudes 46°40′ y 56°30′S. Anales Inst. Patagonia 10, 110–144.
Zhan, L., Chen, L., Zhang, J., Yan, J., Li, Y., Wu, M., Xu, S., Lin, Q., Pan, J., Zhao, J., 2015. Austral summer N_2O sink and source characteristics and their impact factors in Prydz Bay, Antarctica. J. Geophys. Res. Oceans 120, 5836–5849.